

# Four-body dynamics in ${}^6\text{Li}$ elastic scattering

Shin Watanabe,<sup>1,\*</sup> Takuma Matsumoto,<sup>1,†</sup> Kazuyuki Ogata,<sup>2,‡</sup> and Masanobu Yahiro<sup>1,§</sup>

<sup>1</sup>*Department of Physics, Kyushu University, Fukuoka 812-8581, Japan*

<sup>2</sup>*Research Center for Nuclear Physics (RCNP), Osaka University, Ibaraki 567-0047, Japan*

We analyze  ${}^6\text{Li}$  elastic scattering in a wide range of incident energies ( $E_{\text{in}}$ ), assuming the  $n + p + \alpha$  target four-body model and solving the dynamics with the four-body version of the continuum-discretized coupled-channels method (CDCC). Four-body CDCC well reproduces the experimental data with no adjustable parameter for  ${}^6\text{Li} + {}^{209}\text{Bi}$  scattering at  $E_{\text{in}} = 24\text{--}50$  MeV and  ${}^6\text{Li} + {}^{208}\text{Pb}$  scattering at  $E_{\text{in}} = 29\text{--}210$  MeV. In the wide  $E_{\text{in}}$  range,  ${}^6\text{Li}$  breakup is significant and provides repulsive corrections to the folding potential. As an interesting property,  $d$  breakup is strongly suppressed in  ${}^6\text{Li}$ -breakup processes independently of  $E_{\text{in}}$ . We investigate what causes the  $d$ -breakup suppression.

PACS numbers: 24.10.Eq, 25.60.Gc, 25.60.Bx

## I. INTRODUCTION

Understanding of nucleus-nucleus (AA) scattering is a goal in nuclear physics. Recent developments in production of radioactive ion beams make this subject more fruitful. In particular, elastic scattering is an important part of an overall understanding of AA scattering. A widespread approach to this subject such as distorted-wave Born approximation and the continuum discretized coupled-channels method (CDCC) [1–3] is based on the use of an optical potential for the description of elastic scattering. A pioneering systematic analysis on AA elastic scattering was made by Satchler and Love [4, 5]. They found that AA optical potentials, particularly in its real part, can be described by the double-folding model except for weakly-bound projectiles such as  ${}^6\text{Li}$ . The problem on  ${}^6\text{Li}$  scattering was solved later with CDCC by taking account of projectile-breakup effects [1].

Projectile breakup is essential for scattering of weakly-bound nuclei. CDCC is a fully quantum-mechanical method for treating dynamics among various kinds of channels including breakup (continuum) channels. For scattering of deuteron ( $d$ ) on targets (T), the effects are found to be significant in a wide range of incident energies, say  $E_{\text{in}} \lesssim 700$  MeV, by assuming the  $n + p + T$  model and solving the three-body dynamics with CDCC [1]. Nowadays, three-body dynamics in scattering of two-body projectiles is often analyzed by CDCC.

Our interest is now going to four-body dynamics in scattering of three-body projectiles. CDCC for three- and four-body scattering are now called three- and four-body CDCC, respectively. Four-body CDCC is an extension of three-body CDCC, but the formulation is not straightforward since it is not easy to prepare the bound and low-lying continuum states of three-body projectile

before doing coupled-channel calculations. This problem was solved by two approaches; one is the combination [6] of the pseudostate discretization and the complex scaling method [7] and the other is the combination [8] of the momentum-bin discretization and the hyperspherical harmonics method [9]. Four-body CDCC is one of state-of-the-art calculations in nuclear physics.

Three-body projectiles have more complicated structure than two-body ones. A typical and interesting example is the difference between  ${}^6\text{He}$  and  ${}^6\text{Li}$ .  ${}^6\text{He}$  is a Borromean nucleus and is well described by the  $n + n + \alpha$  model.  ${}^6\text{He}$  has no bound state in its two-body subsystems, so that the ground and excited continuum states consist of three-body configurations only. This property makes four-body dynamics of  ${}^6\text{He}$  scattering relatively simpler. Meanwhile,  ${}^6\text{Li}$  is well described by the  $n + p + \alpha$  model and has a bound state in the  $n + p$  subsystem. Therefore, the ground and excited continuum states consist of both  $d\alpha$  two-body and  $np\alpha$  three-body configurations. In fact, the probability of  $d\alpha$  configurations is about 70% in the ground state. This situation makes it more difficult to understand four-body dynamics of  ${}^6\text{Li}$  scattering. Four-body CDCC was first applied to a simpler case, i.e.,  ${}^6\text{He}$  scattering. The analysis was successful in reproducing the experimental data with no adjustable parameter for both elastic and breakup cross sections [6, 8, 10–20].

${}^6\text{Li}$ -breakup effects were first analyzed with three-body CDCC based on the  $d + \alpha + T$  model [1]. This analysis showed that  ${}^6\text{Li}$  breakup effects provide large repulsive corrections to the folding potential. This is the reason why  ${}^6\text{Li}$  elastic scattering was not described by the double-folding model. However, this statement should be reinforced by four-body CDCC.

${}^6\text{Li} + {}^{209}\text{Bi}$  elastic scattering at  $E_{\text{in}} = 29.9$  and 32.8 MeV near the Coulomb-barrier energy  $E_{\text{b}}^{\text{Coul}} \approx 30$  MeV were first analyzed with three-body CDCC [21]; note that  $E_{\text{in}}$  stands for an incident energy in the laboratory system. However, the three-body CDCC calculation could not account for measured elastic cross sections without introducing a normalization factor 0.8 to  $d$ -T and  $\alpha$ -T optical potentials. The problem was solved by four-body

\*s-watanabe@phys.kyushu-u.ac.jp

†matsumoto@phys.kyushu-u.ac.jp

‡kazuyuki@rcnp.osaka-u.ac.jp

§yahiro@phys.kyushu-u.ac.jp

CDCC based on the  $n + p + \alpha + T$  model [22]. In fact, the calculation reproduced the experimental data with no adjustable parameter. As an interesting result, it was reported that  $d$  breakup is strongly suppressed in  ${}^6\text{Li}$  breakup processes of the elastic scattering. The failure of three-body CDCC comes from the use of the phenomenological  $d$ -T optical potential that includes  $d$ -breakup effects implicitly. In fact, if the  $d$ - $\alpha$  potential is replaced by the single folding potential obtained by folding  $p$ -T and  $n$ -T optical potentials with the  $d$  ground state, the three-body CDCC calculation well reproduces the experimental data. Thus, the  $d$ -breakup suppression is a key to understanding four-body dynamics in  ${}^6\text{Li}$  scattering. The next question to be addressed is whether the  $d$ -breakup suppression is realized also at  $E_{\text{in}} > E_{\text{b}}^{\text{Coul}}$ , even if  $d$  breakup is important for the corresponding  $d$  scattering at the same incident energy per nucleon (the same incident velocity) [1].

In this work, four-body ( $n + p + \alpha + \text{target}$ ) dynamics of  ${}^6\text{Li}$  elastic scattering is analyzed over a wide range of  $E_{\text{in}}$  with four-body CDCC. Four-body CDCC reproduces the experimental data without introducing any adjustable parameter for  ${}^6\text{Li} + {}^{209}\text{Bi}$  scattering at  $E_{\text{in}} = 24$ –50 MeV and  ${}^6\text{Li} + {}^{208}\text{Pb}$  scattering at  $E_{\text{in}} = 29$ –210 MeV. We can then investigate the four-body dynamics clearly. In the present  $E_{\text{in}}$  range,  ${}^6\text{Li}$  breakup is significant and provides repulsive corrections to the folding model. The  $d$ -breakup suppression is always realized in the  $E_{\text{in}}$  range. We then investigate what causes the  $d$ -breakup suppression.

In the present work, the theoretical framework consists of four-body CDCC for reaction calculations and the Gaussian expansion method (GEM) [23] for structure calculations. This framework is recapitulated in Sec. II. In Sec. III, we present the results of four-body CDCC calculations and discuss the nature of the  $d$ -breakup suppression. Section IV is devoted to a summary.

## II. THEORETICAL FRAMEWORK

### A. Four-body CDCC

We recapitulate four-body CDCC for  ${}^6\text{Li}$  scattering from a target nucleus (T); see Ref. [3] for the detail. Since  ${}^6\text{Li}$  is well described by the  $n + p + \alpha$  three-body model, we consider the  $n + p + \alpha + T$  four-body system for  ${}^6\text{Li}$  scattering. The scattering state  $\Psi$  with the total energy  $E$  is then governed by the four-body Schrödinger equation

$$(H_4 - E)\Psi = 0, \quad (1)$$

with the total Hamiltonian

$$H_4 = K_{\mathbf{R}} + U_n + U_p + U_\alpha + \frac{e^2 Z_{\text{Li}} Z_{\text{T}}}{R} + h_{np\alpha}, \quad (2)$$

where  $h_{np\alpha}$  denotes the internal Hamiltonian of  ${}^6\text{Li}$ ,  $K_{\mathbf{R}}$  stands for the kinetic energy operator with respect to

the relative coordinate  $\mathbf{R}$  between  ${}^6\text{Li}$  and T, and  $U_x$  ( $x = n, p, \alpha$ ) represents the optical potential between  $x$  and T. In Eq. (2), the Coulomb breakup is neglected and the Coulomb interactions of  $p$ -T and  $\alpha$ -T are then approximated into  $e^2 Z_{\text{Li}} Z_{\text{T}} / R$ , where  $Z_{\text{A}}$  is the atomic number of nucleus A. This approximation is performed in all the calculations except for Fig. 11, and its accuracy is discussed in Appendix A and B.

In CDCC, Eq. (1) is solved in the model space  $P$  spanned by the ground and discretized continuum states that are obtained by diagonalizing  $h_{np\alpha}$  with  $L^2$ -type basis functions:

$$P = \sum_{\gamma=0}^N |\Phi_\gamma\rangle \langle \Phi_\gamma|, \quad (3)$$

where  $\Phi_\gamma$  represents the  $\gamma$ -th eigenstate with an eigenenergy  $\varepsilon_\gamma$ , i.e.,  $\Phi_0$  is the ground state of  ${}^6\text{Li}$  and the  $\Phi_\gamma$  for  $\gamma = 1$ – $N$  mean discretized continuum states of  ${}^6\text{Li}$ . This model-space assumption reduces Eq. (1) to

$$P(H_4 - E)P\Psi_{\text{CDCC}} = 0, \quad (4)$$

for the CDCC wave function

$$\Psi_{\text{CDCC}} = \sum_{\gamma=0}^N \chi_\gamma(\mathbf{R}) |\Phi_\gamma\rangle, \quad (5)$$

where the expansion coefficient  $\chi_\gamma$  describes the relative motion between T and  ${}^6\text{Li}$  in its  $\gamma$ -th state. Equation (4) leads to a set of coupled equations for  $\chi_\gamma$ :

$$[K_{\mathbf{R}} + U_{\gamma\gamma} - (E - \varepsilon_\gamma)]\chi_\gamma(\mathbf{R}) = -U_{\gamma\gamma'}\chi_{\gamma'}(\mathbf{R}), \quad (6)$$

with the coupling potentials

$$U_{\gamma\gamma'} = \langle \Phi_\gamma | U_n + U_p + U_\alpha | \Phi_{\gamma'} \rangle + \frac{e^2 Z_{\text{Li}} Z_{\text{T}}}{R} \delta_{\gamma\gamma'}. \quad (7)$$

This CDCC equation is solved under the standard boundary condition.

### B. Structure of ${}^6\text{Li}$ in GEM

We construct the  $\Phi_\gamma$  by applying the Gaussian expansion method (GEM) [23] to the  $n + p + \alpha$  system. The calculation procedure for  ${}^6\text{Li}$  is the same as that for  ${}^6\text{He}$  in Ref. [12, 16], although the spin-parity of  $\Phi_0$  is  $1^+$  for  ${}^6\text{Li}$  but  $0^+$  for  ${}^6\text{He}$ . In the GEM, three kinds of Jacobi coordinates,  $\xi_c = \{\mathbf{r}_c, \mathbf{y}_c\}$  for  $c = 1$ –3, are taken as shown in Fig. 1. Thanks to this model setting,  ${}^5\text{He}$ - $p$ ,  ${}^5\text{Li}$ - $n$ ,  $d$ - $\alpha$ , and  $n$ - $p$ - $\alpha$  configurations are well incorporated, and thereby fast convergence is obtained with respect to expanding the model space  $P$ .

The model Hamiltonian  $h_{np\alpha}$  is defined by

$$h_{np\alpha} = T_{\mathbf{r}_c} + T_{\mathbf{y}_c} + V_{n\alpha} + V_{p\alpha} + V_{np} + V_{\text{PF}} \quad (8)$$

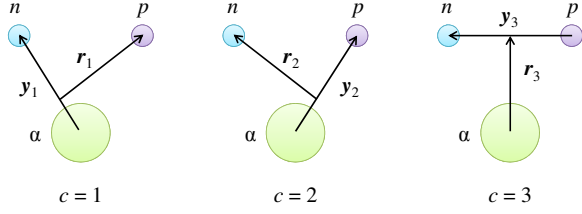


FIG. 1: (Color online) Three sets of Jacobi coordinates  $\xi_c = \{\mathbf{r}_c, \mathbf{y}_c\}$  in the  $n + p + \alpha$  three-body system. Each set is identified by a label  $c$ .

with the kinetic energy operator  $T_{\mathbf{x}}$  of coordinate  $\mathbf{x} = \mathbf{r}_c, \mathbf{y}_c$  and the interaction  $V_{ab}$  between particles a and b. We take the so-called KKNN interaction [24] for  $V_{n\alpha}$  and  $V_{p\alpha}$  and the Bonn-A interaction [25] for  $V_{np}$ . The interactions well reproduce the corresponding low-energy scattering data. The operator

$$V_{\text{PF}} = \lim_{\lambda_{\text{PF}} \rightarrow \infty} \lambda_{\text{PF}} \sum_{c=1}^2 |\phi_{\text{PF}}(\mathbf{y}_c)\rangle \langle \phi_{\text{PF}}(\mathbf{y}_c)| \quad (9)$$

is introduced to exclude the Pauli forbidden states  $\phi_{\text{PF}}$ , where  $\lambda_{\text{PF}} = 10^6$  MeV is taken in actual calculations.

In the GEM, the eigenstates are described as

$$\Phi_{\gamma} \equiv \Phi_{nI^{\pi}}(\xi) = \sum_{c=1}^3 \psi_{nI^{\pi}}^{(c)}(\mathbf{y}_c, \mathbf{r}_c) \quad (10)$$

with the Gaussian basis functions

$$\psi_{nI^{\pi}}^{(c)}(\mathbf{y}_c, \mathbf{r}_c) = \sum_{\lambda\ell\Lambda S} \sum_{i=1}^{i_{\text{max}}} \sum_{j=1}^{j_{\text{max}}} A_{i\lambda j\ell\Lambda S}^{(c)nI^{\pi}} \varphi_{i\lambda j\ell\Lambda S}^{(c)}(\mathbf{y}_c, \mathbf{r}_c), \quad (11)$$

$$\varphi_{i\lambda j\ell\Lambda S}^{(c)}(\mathbf{y}_c, \mathbf{r}_c) = y_c^{\lambda} e^{-(y_c/\bar{y}_i)^2} r_c^{\ell} e^{-(r_c/\bar{r}_j)^2} \times \left[ [Y_{\lambda}(\Omega_{y_c}) \otimes Y_{\ell}(\Omega_{r_c})]_{\Lambda} \otimes [\eta_{1/2}^{(n)} \otimes \eta_{1/2}^{(p)}]_S \right]_{I^{\pi}}, \quad (12)$$

where the index  $i$  ( $j$ ) means the  $i$ -th ( $j$ -th) basis function for the coordinate  $y$  ( $r$ ), the symbol  $\lambda$  ( $\ell$ ) denotes the angular momentum regarding  $\mathbf{y}$  ( $\mathbf{r}$ ), and  $\Lambda$  stands for the total angular momentum. Furthermore,  $\eta_{1/2}^{(n)}$  and  $\eta_{1/2}^{(p)}$  denote the spin wave functions for  $n$  and  $p$ , and the total spin  $S$  of the  $p + n$  system is set to 1. In actual calculations,  $\lambda$  and  $\ell$  are truncated at  $\lambda = \lambda_{\text{max}}$  and  $\ell = \ell_{\text{max}}$ , respectively. The range parameters of Gaussian basis functions are taken in the geometric progression:

$$\bar{y}_i = \bar{y}_1 (\bar{y}_{\text{max}}/\bar{y}_1)^{(i-1)/(i_{\text{max}}-1)}, \quad (13)$$

$$\bar{r}_j = \bar{r}_1 (\bar{r}_{\text{max}}/\bar{r}_1)^{(j-1)/(j_{\text{max}}-1)} \quad (14)$$

with  $i_{\text{max}} = j_{\text{max}} = 10$ . The range parameters ( $\bar{y}_1, \bar{y}_{\text{max}}, \bar{r}_1, \bar{r}_{\text{max}}$ ) are shown in Table I, together with the values of  $\lambda_{\text{max}}$  and  $\ell_{\text{max}}$ .

The effective three-body force

$$V^{3\text{body}}(y_1, y_2) = V_3 e^{-\nu(y_1^2 + y_2^2)} \quad (15)$$

$c$	$I^{\pi}$	$\lambda_{\text{max}}$	$\ell_{\text{max}}$	$\bar{y}_1$ (fm)	$\bar{y}_{\text{max}}$ (fm)	$\bar{r}_1$ (fm)	$\bar{r}_{\text{max}}$ (fm)
3	$1^+$	2	2	0.1	12.0	0.5	12.0
1,2	$1^+$	2	2	0.5	12.0	0.5	12.0
3	$2^+$	3	2	0.1	12.0	0.5	12.0
1,2	$2^+$	2	2	0.5	12.0	0.5	12.0
3	$3^+$	4	2	0.1	12.0	0.5	12.0
3	$3^+$	4	2	0.5	12.0	0.5	12.0

TABLE I: Model space of GEM calculations. The maximum angular momenta and the Gaussian range parameters are presented for each Jacobi coordinate.

is added to  $h_{np\alpha}$  so that the theoretical results can reproduce measured binding energy ( $\varepsilon_0$ ) [26] and root mean square radius ( $R_{\text{rms}}$ ) [27] of  ${}^6\text{Li}$ ; in the present case, the optimal parameter set is  $V_3 = -1.05$  MeV and  $\nu = 0.01$  fm $^{-2}$ . Diagonalizing  $h_{np\alpha} + V^{3\text{body}}$  with the Gaussian basis functions, we obtain the  $\Phi_{\gamma}$ . The theoretical results are summarized in Table II.

	$I^{\pi}$	$\varepsilon_0$ (MeV)	$R_{\text{rms}}$ (fm)
Calc.	$1^+$	-3.69	2.43
Exp.	$1^+$	-3.6989	2.44 $\pm$ 0.07

TABLE II: The spin-parity ( $I^{\pi}$ ), the energy ( $\varepsilon_0$ ) and the matter root mean square radius ( $R_{\text{rms}}$ ) of the  ${}^6\text{Li}$  ground state calculated with the GEM. The experimental data are taken from Refs. [26, 27].

The resultant eigenenergies are illustrated in Fig. 2, together with the  $d + \alpha$  two-body threshold energy  $\varepsilon_{\text{th}}^{(d\alpha)} = -2.2$  MeV and the  $n + p + \alpha$  three-body one  $\varepsilon_{\text{th}}^{(np\alpha)} = 0$  MeV. The ground states and the discretized breakup states of  $1^+, 2^+, 3^+$  with  $\varepsilon < \varepsilon_{\text{max}} = 10$  MeV are taken as the model space  $P$  in CDCC calculations. We confirmed that this model space yields good convergence for the present  ${}^6\text{Li}$  elastic scattering.

### III. RESULTS

#### A. ${}^6\text{Li} + {}^{209}\text{Bi}$ elastic scattering

First,  ${}^6\text{Li} + {}^{209}\text{Bi}$  elastic scattering is analyzed at  $E_{\text{in}} = 24\text{--}50$  MeV with four-body CDCC. As for  $U_n$ , we take the potential of Koning and Delaroche [28], but the spin-orbit interaction is neglected for simplicity. The central potential almost reproduces measured differential cross sections of  $n + {}^{209}\text{Bi}$  scattering at 5 MeV, but the agreement is not perfect. We then made a fine tuning by slightly modifying the parameter set [22]; the resulting parameters are  $a_V = 0.55$  fm,  $W_V = 0$  MeV, and  $W_D = 4.0$  MeV. For simplicity, the same parameter set is taken for all the incident energies, and  $U_p$  is assumed to have the same geometry as  $U_n$ . The potential  $U_{\alpha}$  is taken from

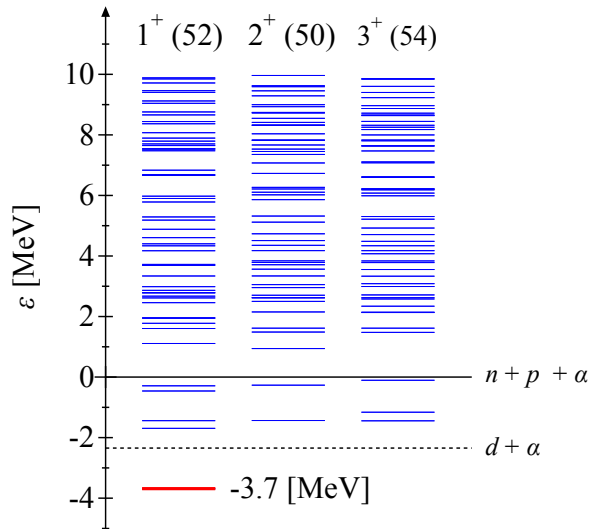


FIG. 2: (Color online) Calculated eigenenergies of  ${}^6\text{Li}$  for  $I^\pi = 1^+, 2^+, \text{ and } 3^+$  from the  $np\alpha$  threshold ( $\varepsilon_{\text{th}}^{(np\alpha)} = 0$  MeV). The  $d\alpha$  threshold ( $\varepsilon_{\text{th}}^{(d\alpha)} = -2.2$  MeV) is also shown by the dotted line. The numbers of pseudostates up to  $\varepsilon_{\text{max}} = 10$  MeV are shown in the parentheses.

Ref. [29] determined from measured differential cross sections of  ${}^4\text{He} + {}^{209}\text{Bi}$  scattering at 19–22 MeV.

Differential cross sections are plotted as a function of scattering angle  $\theta_{\text{cm}}$  in Fig. 3 for  ${}^6\text{Li} + {}^{209}\text{Bi}$  scattering at  $E_{\text{in}} = 32.8\text{--}50$  MeV that is larger than the Coulomb-barrier energy  $E_b^{\text{Coul}} \approx 30$  MeV. The experimental data are taken from Refs. [30–32]. Four-body CDCC calculations (solid lines) reproduce the data with no adjustable parameter. The dashed lines denote the results of one-channel (1ch) calculations with no breakup effect. The difference between the solid and dashed lines is large, indicating that  ${}^6\text{Li}$  breakup, i.e., four-body dynamics is important at  $E_{\text{in}} > V_b$ . The scattering angle  $\theta_r$  at which the dashed line becomes maximum nearly corresponds to a rainbow angle in a semi-classical picture, and the scattering angle  $\theta_g$  at which the Rutherford ratio is 1/4 approximately corresponds to a grazing angle.  ${}^6\text{Li}$ -breakup effects suppress a strong diffraction pattern of the dashed line at  $\theta_{\text{cm}}$  around  $\theta_r$  and enhances the cross section largely at  $\theta_{\text{cm}}$  around  $\theta_g$ ; see Fig. 3(a) for the suppression and Fig. 3(b) for the enhancement.

Figure 4 shows the same figure as Fig. 3, but  $E_{\text{in}}$  is smaller than  $V_b$ . Again, four-body CDCC calculations well account for measured differential cross sections.  ${}^6\text{Li}$  breakup effects become small as  $E_{\text{in}}$  decreases from  $V_b$ . In contrast, for the total reaction cross section  $\sigma_R$ , the effects are more significant as  $E_{\text{in}}$  goes down from  $V_b$ , as shown in Fig. 5. Four-body dynamics is thus essential for both  $E_{\text{in}} < V_b$  and  $E_{\text{in}} > V_b$ .

${}^6\text{Li} + {}^{209}\text{Bi}$  scattering at  $E_{\text{in}} = 29.9$  and 32.8 MeV were already analyzed by four-body CDCC in our previous work [22]. The present calculations are improved from the previous one at the following two points. In the

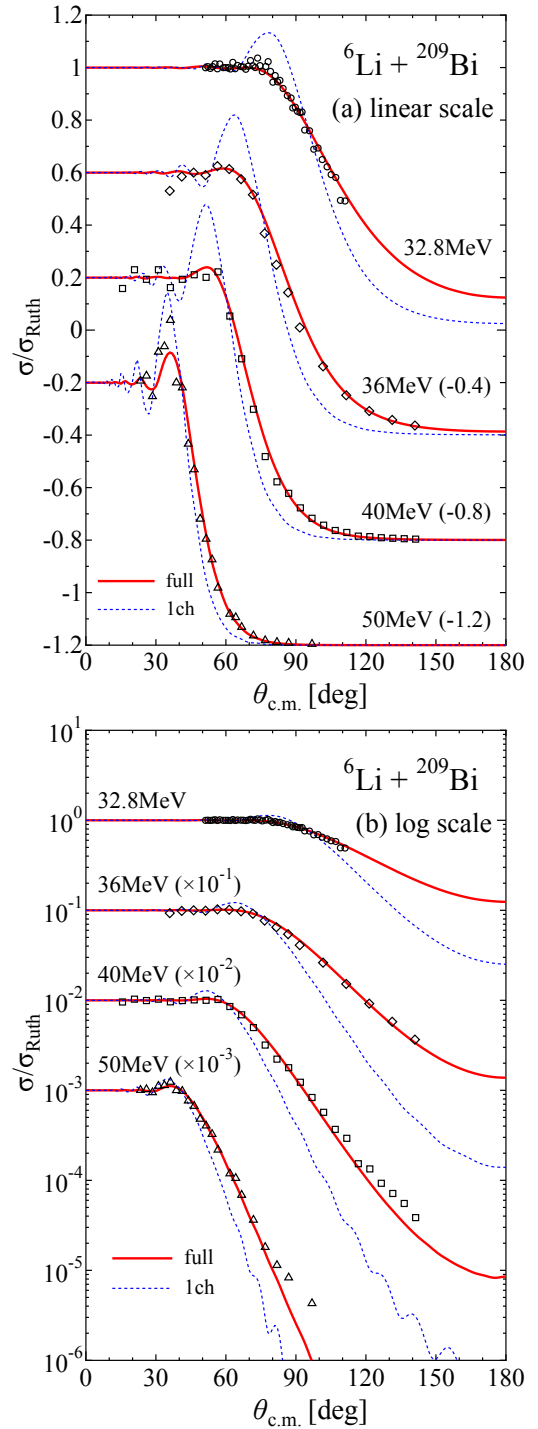


FIG. 3: (Color online) Elastic cross sections (normalized by the Rutherford cross section) for  ${}^6\text{Li} + {}^{209}\text{Bi}$  scattering at 32.8–50 MeV in (a) the linear scale and (b) the logarithmic scale. The solid lines represent the results of full four-body CDCC calculations, whereas the dotted lines show the results of 1ch calculations with no breakup effect. The symbols are experimental data taken from Refs. [30–32].

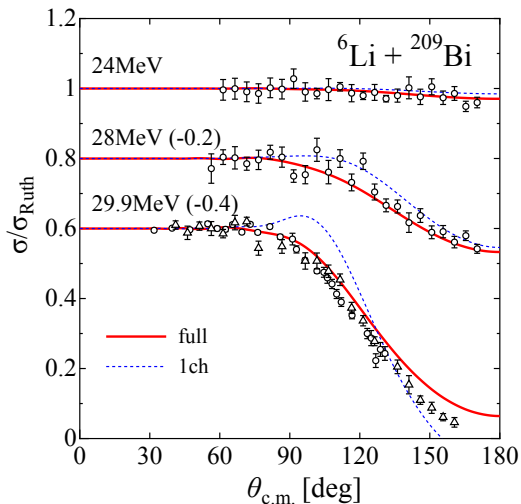


FIG. 4: (Color online) Same as Fig. 3, but  $E_{\text{in}} = 24, 28$  and  $29.9$  MeV.

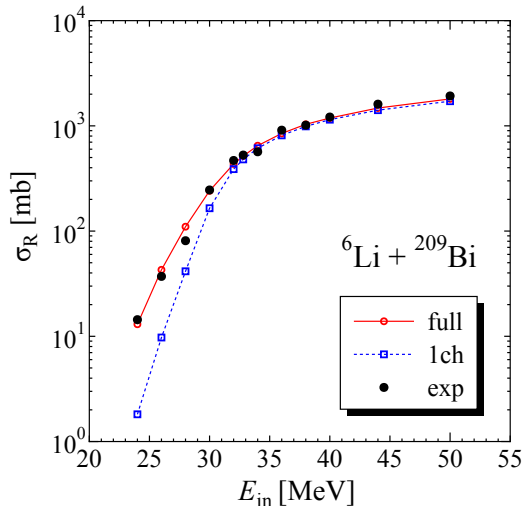


FIG. 5: (Color online) Total reaction cross section  $\sigma_{\text{R}}$  as a function of  $E_{\text{in}}$ . The solid and dotted line represents the calculation with and without the channel coupling effects. The derived cross section based on the optical model analysis [32] is also shown.

previous work, the matter radius  $R_{\text{rms}}$  of  ${}^6\text{Li}$  was 2.34 fm and slightly underestimates the experimental data  $R_{\text{rms}} = 2.44 \pm 0.07$  fm. This problem is solved by taking a different parameter set for  $V^{3\text{body}}$ ; in the present case  $R_{\text{rms}} = 2.43$  fm, as shown in Table II. The second point is the accuracy of numerical calculations. In the previous work, the diagonal potentials  $U_{\gamma\gamma}$  between  $2^+$  breakup states were numerically inaccurate. This problem is also solved. These two corrections are small, so that the present results are very close to the previous ones.

## B. ${}^6\text{Li} + {}^{208}\text{Pb}$ elastic scattering

We make the same analysis for a  ${}^{208}\text{Pb}$  target, since the experimental data are available up to the high incident energy of  $E_{\text{in}} = 210$  MeV. Again, we take the central part of the Koning-Delaroche potential for  $U_n$ , and as  $U_\alpha$  we use the optical potentials of Ref. [29] for  $E_{\text{in}} = 29$  and 39 MeV and those of Ref. [33] for  $E_{\text{in}} = 73.7$  and 210 MeV; note that  $U_p$  has the same geometry as  $U_n$ .

Figure 6 shows the angular distribution of elastic cross sections for  ${}^6\text{Li} + {}^{208}\text{Pb}$  scattering at  $E_{\text{in}} = 29, 39, 73.7$  and 210 MeV. The experimental data are taken from Refs [34–36]. This scattering are also well explained by four-body CDCC over a wide range of  $E_{\text{in}} = 29$ –210 MeV in virtue of projectile-breakup effects.

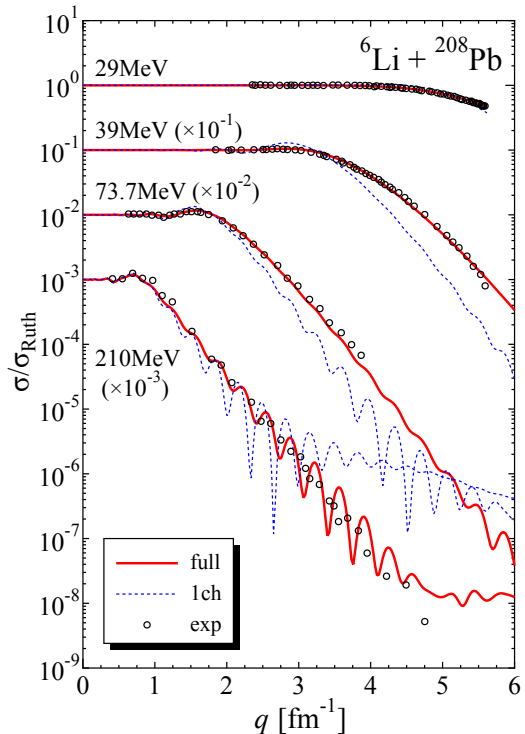


FIG. 6: (Color online) Elastic cross sections (normalized by the Rutherford cross section) for  ${}^6\text{Li} + {}^{208}\text{Pb}$  scattering at 29–210 MeV as a function of the transfer momentum  $q$ . The solid lines represent the results of full four-body CDCC calculations, whereas the dotted lines denote the results of 1ch calculations. The experimental data are taken from Refs. [34–36].

We discuss the elastic  $S$ -matrix elements in Fig. 7 for  ${}^6\text{Li} + {}^{208}\text{Pb}$  scattering at  $E_{\text{in}} = 39$  and 210 MeV. The elements are represented by  $S_{L'L}^{(J)}$ , where  $J$  is the total angular momentum and  $L$  ( $L'$ ) is the initial (final) angular momentum regarding  $\mathbf{R}$  satisfying the relations  $|J-1| \leq L \leq J+1$  and  $|J-1| \leq L' \leq J+1$ . Only the diagonal elements  $S_{JJ}^{(J)}$  are plotted as a function of  $J$  in Fig. 7. Closed circles connected with solid lines (open squares connected with dotted lines) stand for the results

of full-CDCC (1ch) calculations. Projectile breakup effects become small as  $E_{\text{in}}$  increases from 39 MeV to 210 MeV, but the effects are still not negligible at  $E_{\text{in}} = 210$  MeV, as shown in Fig. 6. Projectile-breakup effects rotate  $S_{JJ}^{(J)}$  clockwise at the grazing total angular momentum  $J_{\text{gr}}$ ; note that  $J_{\text{gr}} = 17$  for 39 MeV and 69 for 210 MeV. The effects thus provide repulsive corrections to the results of 1ch calculations, i.e., the folding potential. This result is consistent with that of Ref. [1] based on three-body CDCC.

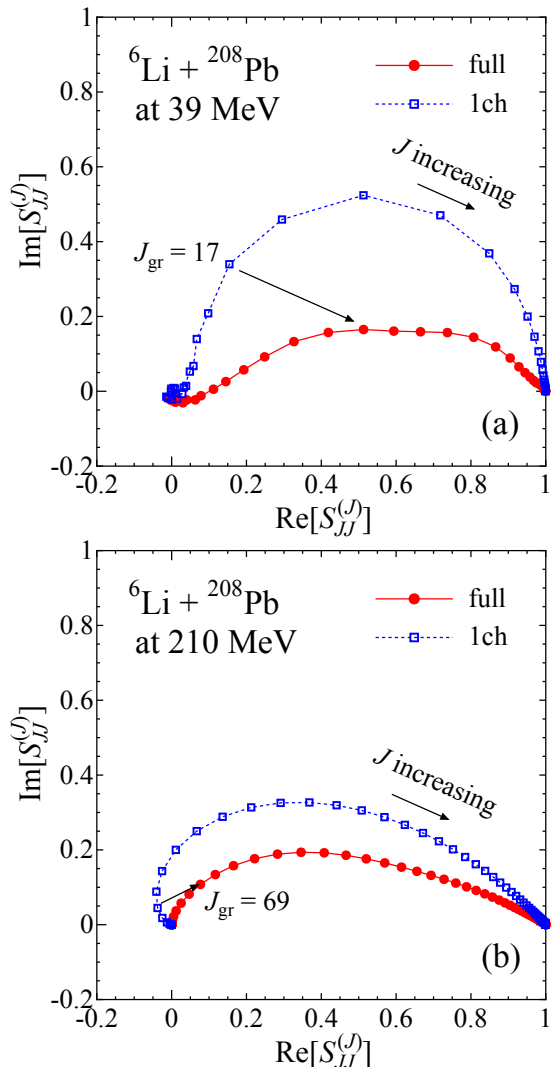


FIG. 7: (Color online) Elastic  $S$ -matrix elements for  ${}^6\text{Li} + {}^{208}\text{Pb}$  scattering (a) at  $E_{\text{in}} = 39$  MeV and (b) at  $E_{\text{in}} = 210$  MeV. The open circles stand for the results of full CDCC calculations, and the closed squares correspond to the results of 1ch calculations.

### C. Four- and three-body dynamics

In general, the ground and breakup states of  ${}^6\text{Li}$  consist of  $d\alpha$  (two-body) and  $np\alpha$  (three-body) configurations, although the main component of the ground state is a  $d\alpha$  one. It is found in our previous paper [22] that  $d$  little breaks up in  ${}^6\text{Li}$ -breakup processes of  ${}^6\text{Li} + {}^{209}\text{Bi}$  elastic scattering at  $E_{\text{in}} \approx E_{\text{b}}^{\text{Coul}} (\approx 30 \text{ MeV})$ . In this subsection, we confirm that the  $d$ -breakup suppression ( $d\alpha$  dominance) in  ${}^6\text{Li}$  elastic scattering is realized also for  $E_{\text{b}}^{\text{Coul}} < E_{\text{in}} \lesssim 210$  MeV. When  ${}^6\text{Li}$  elastic scattering is compared with  $d$  one at the same incident energy per nucleon (the same incident velocity),  $d$  breakup is strongly suppressed in the former scattering but not in the latter one. Note that in  $d$  scattering  $d$  breakup is significant at incident energies up to 700 MeV [1].

The model space  $P$  of CDCC calculations can be decomposed into the ground-state part  $P_0$  and the breakup-state part  $P^*$  as  $P = P_0 + P^*$  for

$$P_0 = |\Phi_0\rangle \langle \Phi_0|, \quad P^* = \sum_{\gamma=1}^N |\Phi_\gamma\rangle \langle \Phi_\gamma|. \quad (16)$$

For later discussion,  $P^*$  is further divided into a subspace  $P_{np\alpha}$  dominated by  $np\alpha$  configurations and a subspace  $P_{d\alpha}$  by  $d\alpha$  configurations. The subspaces are defined as follows. The probability of  $d\alpha$  configurations in the breakup state  $\Phi_\gamma$  is obtained by the overlap between  $\Phi_\gamma$  and the  $d$  ground state  $\phi^{(d)}$ :

$$\Gamma_\gamma^{(d\alpha)} = \left| \langle \phi^{(d)}(\mathbf{y}) | \Phi_\gamma(\mathbf{y}, \mathbf{r}) \rangle \right|^2. \quad (17)$$

We then define a breakup state with  $\Gamma_\gamma^{(d\alpha)} > 0.5$  ( $\Gamma_\gamma^{(d\alpha)} \leq 0.5$ ) as a  $d\alpha$ -dominant ( $np\alpha$ -dominant) state. The subspace  $P_{d\alpha}$  ( $P_{np\alpha}$ ) is a model space spanned by  $d\alpha$ -dominant ( $np\alpha$ -dominant) breakup states. Consequently, the model space  $P$  of CDCC calculations is expressed as

$$P = P_0 + P_{d\alpha} + P_{np\alpha}. \quad (18)$$

In the present calculation, the  $d\alpha$  probability  $\Gamma_0^{(d\alpha)}$  for the  ${}^6\text{Li}$  ground state is 0.70 and the corresponding spectroscopic overlap  $(\Gamma_0^{(d\alpha)})^{1/2}$  is 0.83. This result is consistent with the value 0.86 of other three-body model calculation [37] and the experimental estimation  $0.85 \pm 0.04$  [38]. The  ${}^6\text{Li}$  ground state is thus one of  $d\alpha$  dominant states. The numbers of  $np\alpha$ - and  $d\alpha$ -dominant states in the  $P^*$  space are 140 and 15, respectively, i.e.,  $P_{np\alpha}$  is much larger than  $P_{d\alpha}$ . This comes from the fact that the three-body phase space is larger than the two-body one.

Now we confirm that the  $d$ -breakup suppression is realized also for  ${}^6\text{Li}$  scattering at  $E_{\text{in}} > E_{\text{b}}^{\text{Coul}}$ . Figure 8 shows differential cross sections for  ${}^6\text{Li} + {}^{208}\text{Pb}$  scattering at  $E_{\text{in}} = 39$  and 210 MeV. The solid and dotted lines are the same as in Fig. 6. When  $d\alpha$ -dominant states are switched off from full-CDCC calculations (solid line), we

get the dot-dashed line. The line is close to the result of 1ch calculations (dotted line) for each of  $E_{\text{in}} = 39$  and 210 MeV. Figure 9 is the same as Fig. 8, but  $np\alpha$ -dominant states are switched off from full-CDCC calculations (solid line). The result (dot-dashed line) is close to the result of full-CDCC calculations (solid line). The  $d\alpha$  dominance ( $d$ -breakup suppression) in  ${}^6\text{Li}$  breakup is thus confirmed.

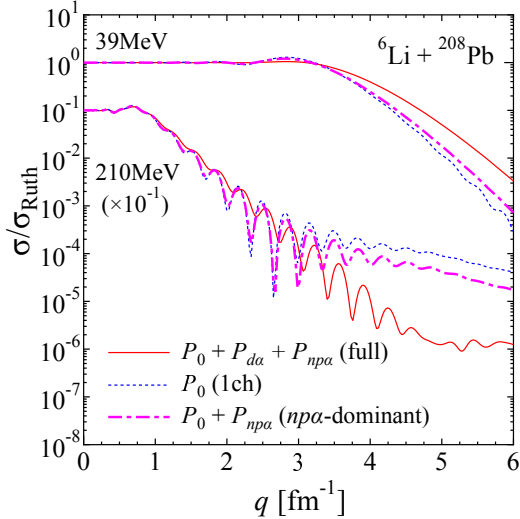


FIG. 8: (Color online) Elastic cross sections (normalized by the Rutherford cross section) for  ${}^6\text{Li} + {}^{208}\text{Pb}$  scattering at  $E_{\text{in}} = 39$  and 210 MeV. The solid line represents the result of full four-body CDCC calculations, whereas the dotted line denotes the results of 1ch calculations with no breakup channel. In the dot-dashed line, the model space  $P_{d\alpha}$  is switched off from the solid line.

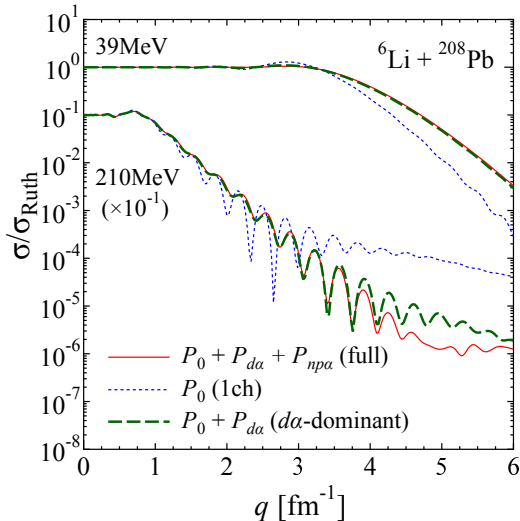


FIG. 9: (Color online) Same as Fig 8, but in the dot-dashed line the model space  $P_{np\alpha}$  is switched off from the solid line.

In order to understand the nature of the  $d\alpha$  dominance, we plot the  $\Gamma_\gamma^{(d\alpha)}$  as a function of  $\varepsilon$  in Fig. 10. In

the region  $\varepsilon_{\text{th}}^{(d\alpha)} < \varepsilon < \varepsilon_{\text{th}}^{(np\alpha)}$ , the  $\Gamma_\gamma^{(d\alpha)}$  are even larger than  $\Gamma_0^{(d\alpha)} = 0.70$ . The  $d\alpha$  dominance is thus somewhat developed in this region. Above  $\varepsilon_{\text{th}}^{(np\alpha)}$ , some low-lying states keep  $P_\gamma^{(d\alpha)}$  large; in fact, the values are comparable to  $\Gamma_0^{(d\alpha)}$ . Eventually, some of 15  $d\alpha$ -dominant breakup states are concentrated on the low-lying part of excitation spectrum near  $\varepsilon_{\text{th}}^{(np\alpha)}$ , whereas 140  $np\alpha$ -dominant breakup states spread out in the spectrum.

The  $d\alpha$ -dominant breakup states are thus located in the lowlying part of excitation spectrum, because the only  $n + p$  subsystem has a bound state. Therefore, the low-lying  $d\alpha$ -dominant breakup states can work as a collective mode, since the breakup states have structures similar to the  ${}^6\text{Li}$  ground state and the transitions between them become strong. In fact, the coupling potentials  $U_{\gamma 0}$  from the ground state to the low-lying  $d\alpha$ -dominant states are much larger than the  $U_{\gamma 0}$  to the  $np\alpha$ -dominant breakup states. This property means that the incident flux in the elastic channel mainly goes to the low-lying  $d\alpha$ -dominant breakup channels and comes back to the elastic channel. This is the reason why the  $d\alpha$  dominance ( $d$ -breakup suppression) is realized in  ${}^6\text{Li}$  breakup independently of  $E_{\text{in}}$ .

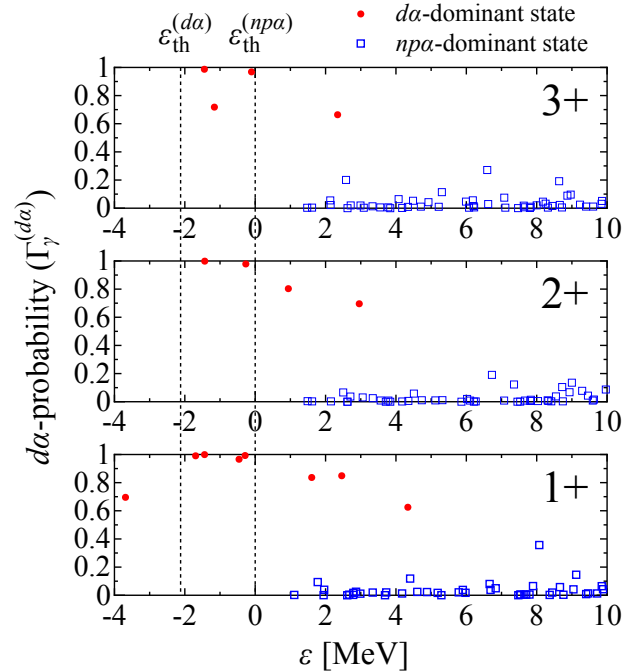


FIG. 10: (Color online) Distribution of  $d\alpha$ -probability in excitation spectrum. The closed circles (open squares) correspond to the  $d\alpha$ -dominant states ( $np\alpha$ -dominant states); see text for details. The threshold energies of  $\varepsilon_{\text{th}}^{(d\alpha)} = -2.2$  MeV and  $\varepsilon_{\text{th}}^{(np\alpha)} = 0$  MeV are also shown as the dotted line for reference.

#### IV. SUMMARY

Four-body ( $n + p + \alpha + \text{target}$ ) dynamics of  ${}^6\text{Li}$  elastic scattering was analyzed over a wide range of  $E_{\text{in}}$  with four-body CDCC. Four-body CDCC well reproduced measured elastic and total reaction cross sections with no adjustable parameter for  ${}^6\text{Li} + {}^{209}\text{Bi}$  scattering at  $E_{\text{in}} = 24\text{--}50$  MeV and  ${}^6\text{Li} + {}^{208}\text{Pb}$  scattering at  $E_{\text{in}} = 29\text{--}210$  MeV. In the wide  $E_{\text{in}}$  range,  ${}^6\text{Li}$  breakup is significant and provides repulsive corrections to the folding potential. The problem addressed by Satchler and Love is thus clearly solved by the present four-body CDCC calculation.

In our previous work [22], we found that  $d$  breakup is strongly suppressed in  ${}^6\text{Li}$  scattering near the Coulomb-barrier energy. In the present paper, we confirmed that the  $d$ -breakup suppression is realized for any  $E_{\text{in}}$ , as far as  ${}^6\text{Li}$  breakup itself is significant. This mechanism can be understood as follows. Some of  $d\alpha$ -dominant breakup states are concentrated on the low-lying part of excitation spectrum and work as a collective-excitation mode effectively. In fact,  ${}^6\text{Li}$  breakup is mainly induced by strong transitions to the breakup states, and consequently,  $d$  breakup is suppressed in  ${}^6\text{Li}$  breakup processes.

The  $d$ -breakup suppression may indicate that  ${}^6\text{Li}$  scattering is described effectively by the  $d + \alpha + T$  three-body model, if the following two points are satisfied. As for the potential between  $d$  and  $T$ , we should use the single-folding potential obtained by folding  $U_n$  and  $U_p$  with the  $d$  ground state, since the folding potential does not include  $d$ -breakup effects. As for the projectile ( ${}^6\text{Li}$ ) radius important for elastic scattering, the value calculated with the  $d + \alpha$  two-body model should be consistent with that with the  $n + p + \alpha$  three-body model. A successful example is shown in our previous paper [22]. Further analyses along this line are quite interesting.

#### Acknowledgements

The authors are grateful to K. Minomo and A. M. Moro for fruitful discussions. This work was supported by JSPS KAKENHI Grant Numbers 25-4319, 25400255, 26400278.

#### Appendix A: Coulomb-breakup effects

Here, we check Coulomb-breakup effects on  ${}^6\text{Li} + {}^{209}\text{Bi}$  elastic scattering. In Eq. (2), the Coulomb interaction is then replaced back to

$$\frac{e^2 Z_{\text{Li}} Z_{\text{T}}}{R} \rightarrow \frac{e^2 Z_p Z_{\text{T}}}{R_p} + \frac{e^2 Z_\alpha Z_{\text{T}}}{R_\alpha}. \quad (\text{A1})$$

Figure 11 shows Coulomb-breakup effects on differential cross sections for  ${}^6\text{Li} + {}^{209}\text{Bi}$  elastic scattering at

$E_{\text{in}} = 28\text{--}50$  MeV. The solid and dashed lines correspond to CDCC calculations without and with Coulomb breakup, respectively. The difference between the two lines is tiny, indicating that Coulomb-breakup effects are quite small. This comes from the lack of electric dipole transitions; see Appendix B for the theoretical discussion. Coulomb breakup effects are thus suppressed in  ${}^6\text{Li}$  elastic scattering compared with  ${}^6\text{He}$  scattering [16, 21].

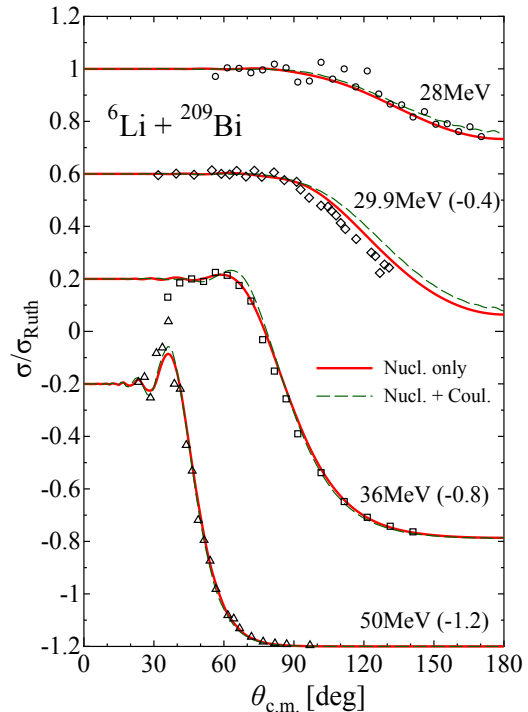


FIG. 11: (Color online) Coulomb-breakup effects on  ${}^6\text{Li} + {}^{209}\text{Bi}$  elastic cross section at 28–50 MeV. The solid and dashed lines show the results of CDCC calculations without and with Coulomb breakup. The symbols are experimental data taken from Refs. [30–32].

#### Appendix B: Electric dipole transitions in the $N + N + \alpha$ three-cluster model

Coulomb breakup is mainly induced by the electric dipole transition. It is well known that the transition strength vanishes in the  $d + \alpha$  model for  ${}^6\text{Li}$ , since the mass ratio  $m_d/m_\alpha$  equals to the charge one  $Z_d/Z_\alpha$  [21, 39]. The vanishment is true also for the  $n + p + \alpha$  model, as shown later. Let us consider the  $N + N + \alpha$  three-cluster model illustrated in Fig. 12 in which two nucleons are labeled by 1 and 2 and  ${}^4\text{He}$  is by 3. In the model, the dipole operator ( $D_\mu$ ) is given by

$$D_\mu = \sum_{i=1}^2 (1/2 - \tau_{iz}) e x_i Y_{1\mu}(\hat{x}_i) + 2 e x_3 Y_{1\mu}(\hat{x}_3), \quad (\text{B1})$$



where  $\tau_{iz} = 1/2$  ( $-1/2$ ) for  $N = n$  ( $p$ ), and  $\mathbf{x}_i$  is the coordinate of cluster  $i$  from the center of mass ( $G$ ):

$$\mathbf{x}_1 = \frac{2}{3}\mathbf{r} + \frac{1}{2}\mathbf{y}, \quad (\text{B2})$$

$$\mathbf{x}_2 = \frac{2}{3}\mathbf{r} - \frac{1}{2}\mathbf{y}, \quad (\text{B3})$$

$$\mathbf{x}_3 = -\frac{1}{3}\mathbf{r}. \quad (\text{B4})$$

The total isospin  $T$  and its  $z$  component  $T_z$  of  ${}^6\text{Li}$  are zero, and the isospin component of the  ${}^6\text{Li}$  ground state is described by

$$|TT_z\rangle = |00\rangle = \frac{1}{\sqrt{2}}(|np\rangle + |pn\rangle). \quad (\text{B5})$$

The expectation value of  $D_\mu$  for  $|00\rangle$  is then

$$\langle 00|D_\mu|00\rangle = \frac{e}{2} \sum_{i=1}^2 x_i Y_{1\mu}(\hat{\mathbf{x}}_i) + 2ex_3 Y_{1\mu}(\hat{\mathbf{x}}_3) = 0, \quad (\text{B6})$$

since

$$x_1 Y_{1\mu}(\hat{\mathbf{x}}_1) = \frac{2}{3}r Y_{1\mu}(\hat{\mathbf{r}}) + \frac{1}{2}y Y_{1\mu}(\hat{\mathbf{y}}), \quad (\text{B7})$$

$$x_2 Y_{1\mu}(\hat{\mathbf{x}}_2) = \frac{2}{3}r Y_{1\mu}(\hat{\mathbf{r}}) - \frac{1}{2}y Y_{1\mu}(\hat{\mathbf{y}}), \quad (\text{B8})$$

$$x_3 Y_{1\mu}(\hat{\mathbf{x}}_3) = -\frac{1}{3}r Y_{1\mu}(\hat{\mathbf{r}}). \quad (\text{B9})$$

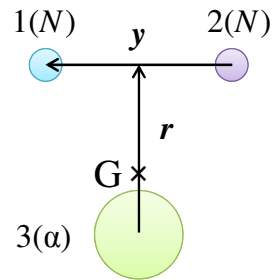


FIG. 12: (Color online) The  $N + N + \alpha$  three-cluster model and its coordinates.

- 
- [1] M. Kamimura, M. Yahiro, Y. Iseri, Y. Sakuragi, H. Kameyama, and M. Kawai, *Prog. Theor. Phys. Suppl.* **89**, 1 (1986).
- [2] N. Austern, Y. Iseri, M. Kamimura, M. Kawai, G. Rawitscher, and M. Yahiro, *Phys. Rep.* **154**, 125 (1987).
- [3] M. Yahiro, K. Ogata, T. Matsumoto, and K. Minomo, *Prog. Theor. Exp. Phys.* **2012**, 01A206 (2012).
- [4] G. R. Satchler and W. G. Love, *Phys. Rep.* **55**, 183 (1979).
- [5] G. R. Satchler, “Direct Nuclear Reactions”, Oxford University Press, (1983).
- [6] T. Matsumoto, K. Katō, and M. Yahiro, *Phys. Rev. C* **82**, 051602(R) (2010).
- [7] J. Aguilar and J.M. Combes, *Commun. Math. Phys.*, **22**, 1971, 269. E. Balslev and J.M. Combes, *Commun. Math. Phys.*, **22**, 1971, 280.
- [8] M. Rodríguez-Gallardo, J. M. Arias, J. Gómez-Camacho, A. M. Moro, I. J. Thompson, and J. A. Tostevin, *Phys. Rev. C* **80**, 051601(R) (2009).
- [9] I. J. Thompson, F. M. Nunes, and B. V. Danilin, *Comput. Phys. Commun.* **161**, 87 (2004).
- [10] A. M. Moro, J. M. Arias, J. Gómez-Camacho, I. Martel, F. Pérez-Bernal, R. Crespo, and F. Nunes, *Phys. Rev. C* **65**, 011602(R) (2001).
- [11] T. Matsumoto, T. Kamizato, K. Ogata, Y. Iseri, E. Hiyama, M. Kamimura, and M. Yahiro, *Phys. Rev. C* **68**, 064607 (2003).
- [12] T. Matsumoto, E. Hiyama, K. Ogata, Y. Iseri, M. Kamimura, S. Chiba, and M. Yahiro, *Phys. Rev. C* **70**, 061601(R) (2004).
- [13] T. Egami, K. Ogata, T. Matsumoto, Y. Iseri, M. Kamimura, and M. Yahiro, *Phys. Rev. C* **70**, 047604 (2004).
- [14] M. Rodríguez-Gallardo, J. M. Arias, J. Gómez-Camacho, A. M. Moro, I. J. Thompson, and J. A. Tostevin, *Phys. Rev. C* **72**, 024007 (2005).
- [15] A. M. Moro, F. Pérez-Bernal, J. M. Arias, and J. Gómez-Camacho, *Phys. Rev. C* **73**, 044612 (2006).
- [16] T. Matsumoto, T. Egami, K. Ogata, Y. Iseri, M. Kamimura, and M. Yahiro, *Phys. Rev. C* **73**, 051602(R) (2006).
- [17] M. Rodríguez-Gallardo, J. M. Arias, J. Gómez-Camacho, R. C. Johnson, A. M. Moro, I. J. Thompson, and J. A. Tostevin, *Phys. Rev. C* **77**, 064609 (2008).
- [18] A. M. Moro, J. M. Arias, J. Gómez-Camacho, and F. Pérez-Bernal, *Phys. Rev. C* **80**, 054605 (2009).
- [19] T. Egami, T. Matsumoto, K. Ogata, and M. Yahiro, *Prog. Theor. Phys.* **121**, 789 (2009).
- [20] T. Matsumoto, T. Egami, K. Ogata, and M. Yahiro, *Prog. Theor. Phys.* **121**, 885 (2009).
- [21] N. Keeley, J. M. Cook, K. W. Kemper, B. T. Roeder, W. D. Weintraub, F. Maréchal, and K. Rusek, *Phys. Rev. C* **68**, 054601 (2003).
- [22] S. Watanabe, T. Matsumoto, K. Minomo, K. Ogata, and

- M. Yahiro, Phys. Rev. C **86**, 031601(R) (2012).
- [23] E. Hiyama, Y. Kino, and M. Kamimura, Prog. Part. Nucl. Phys. **51**, 223 (2003).
- [24] H. Kanada, T. Kaneko, S. Nagata, and M. Nomoto, Prog. Theor. Phys. **61**, 1327 (1979).
- [25] R. Machleidt, Adv. Nucl. Phys. **19**, 189 (1989).
- [26] D. R. Tilley *et al.*, Nucl. Phys. A **708**, 3 (2002).
- [27] A. V. Dobrovolsky *et al.*, Nucl. Phys. A **766**, 1 (2006).
- [28] A. J. Koning and J. P. Delaroche, Nucl. Phys. A **713**, 231 (2003).
- [29] A. R. Barnett and J. S. Lilley, Phys. Rev. C **9**, 2010 (1974).
- [30] E. F. Aguilera *et al.*, Phys. Rev. Lett. **84**, 5058 (2000).
- [31] E. F. Aguilera *et al.*, Phys. Rev. C **63**, 061603 (2001).
- [32] S. Santra *et al.*, Phys. Rev. C **83**, 034616 (2011).
- [33] C. M. Perey and F. G. Perey, Atomic Data and Nuclear Data Tables **17**, 1 (1976).
- [34] N. Keeley *et al.*, Nucl. Phys. A **571**, 326 (1994).
- [35] R. Huffman, A. Galonsky, R. Markham, and C. Williamson, Phys. Rev. C **22**, 1522 (1980).
- [36] A. Nadasen *et al.*, Phys. Rev. C **39**, 536 (1989).
- [37] Y. Kikuchi *et al.*, Phys. Rev. C **84**, 064610 (2011).
- [38] D. R. Tilley, C. M. Cheves, J. L. Grodwin *et al.*, Nucl. Phys. A **708**, 3 (2002).
- [39] B. Buck and A. A. Pilt, Nucl. Phys. A **280**, 133 (1977).